

C hannel Interference in a Q uasi B allistic A haronov-B ohm E xperiment

G . Cemicchiaro^{1,4}, T . M artin², K . Hasselbach¹, D . M ailly³, A . Benoit¹¹ CRTBT-CNRS, 25 av des M artyrs, 38042 G renoble, France² CPT -U niversité d'A ix-M arseille II, 163 av de Lum iny, 13288 M arseille, France³ LMM-CNRS, 196 av. H . Raver, 92220 B agneux, France⁴ CBPF-CNPG, 150 av. Xavier Sigaud, 22000 Rio de Janeiro, Brazil

New experiments are presented on the transmission of electron waves through a 2D EG (2 dimensional electron gas) ring with a gate on top of one of the branches. Magnetoconductance oscillations are observed, and the phase of the Aharonov-Bohm signal alternates between 0 and π as the gate voltage is scanned. A Fourier transform of the data reveals a dominant period in the voltage which corresponds to the energy spacing between successive transverse modes. A theoretical model including random phase shifts between successive modes reproduces the essential features of the experiment.

ment is varied. The essential features of the data can be interpreted using the scattering formulation of quantum transport [4]. The inclusion of disorder is necessary to explain the alternation of AB phases.

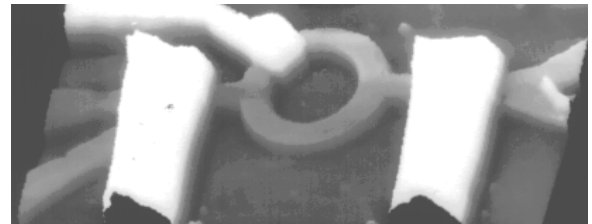


FIG . 1. A tom ic force microscope image: detail of a sample with the gate (white regions) over the upper branch and the gates for the leads.

The Aharonov-Bohm (AB) effect has proven to be an invaluable tool for quantifying interference phenomena in mesoscopic physics. Early experiments on long metal cylinders [1] revealed that an electron accumulates a phase $\Delta\phi$ as it is scattered elastically by impurities while traveling around the loop: when the magnetic flux is varied, an oscillatory pattern with periodicity $h=2e$ results from the interference of an electron wave with its time reversed path [2]. Experiments on gold loops [3] confirmed that for normal metals which are laterally confined, the expected periodicity [4] is that of the single

flux quantum $\phi_0 = h/e$. The amplitude of the magnetoresistance background can be understood within the framework of universal conductance fluctuations (UCF) [5]. The two dimensional electron gas (2D EG) formed at the heterojunction between two semiconductors is used for experiments in the ballistic transport regime. Recently, two experiments on gated rings in the diusive [6], and the ballistic [7] regime reported oscillations associated with the modulation of the electron wave length under the gate.

In the present letter, results on a new AB transport measurement in the ballistic regime are exposed. The number of lateral channels in one branch of the ring is adjusted by means of an electrostatic gate. In addition to the usual AB interference, a periodic pattern is uncovered when the number of lateral electron modes is modulated with the gate. It is emphasized that the conductance pattern contains two types of oscillations: a) the wavelength variation under the gate [6,7], and b) a "new" periodicity associated with the closing/opening of transverse modes in the ring. Phase switching and period halving in the AB pattern is monitored as the con-

The 2D electron gas was created at the interface of a GaAs/GaAs heterojunction. Via standard electron beam lithography [8] a single loop device of width 1.2 μm with inner diameter 4 μm , connected to measurement leads was designed (Fig. 1). In this etched structure, the width of the wire which constitutes the ring is further reduced by a depletion on each edge of 0.27 μm . The 2D EG presents a mobility of $1.14 \times 10^6 \text{ cm}^2/\text{Vs}$, an electron density of $n_s = 3.6 \times 10^{11} \text{ cm}^{-2}$. The coherence length $l_c > 20 \mu\text{m}$ and the mean free path $l_e = 11.3 \mu\text{m}$, are consistent with the ballistic regime. A metallic gate was deposited over one branch of the ring (hereby referred to as the upper branch) allowing a controlled depletion of the 2D EG underneath. The number of electron channels N in the wires defining the ring is estimated assuming parabolic confinement in the transverse direction. The width W of the channel roughly equals the ratio of the 1D to the 2D electron density [9]. For $W = 600 \text{ nm}$, and a Fermi wave length $\lambda_F = 40 \text{ nm}$, $N = (3\pi/4)W = \lambda_F^{-2} = 30$ channels. The lateral dimensions of the wire are comparable to that of the conductance quantization experiments [10], where the number of transited channels was shown to scale linearly with the depletion voltage.

The conductance is determined using standard synchronous detection measurements in a four terminal configuration. A low-frequency AC current of 10 nA was injected and measurements were taken at 15 mK, in a dilution refrigerator. An external flux variation of 12 gauss was applied corresponding to 4 flux quanta in the mean radius of the ring. While lowering the gate voltage from

0 to -300 mV by 1 mV steps, the complete conductance pattern was measured over a period of 4 hours. Digital filtering routines were applied to reduce base line variations due to UCFs.

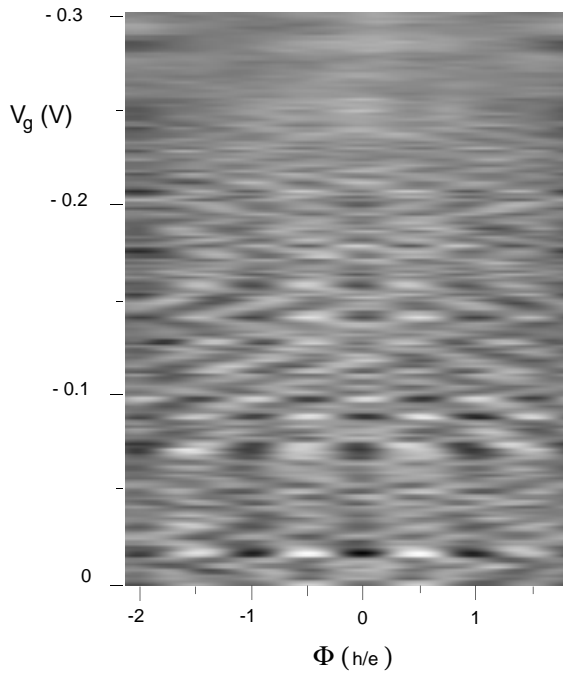


FIG. 2. AB component of the conductance, measured as a function of applied flux (horizontal axis) and gate voltage (vertical axis). Areas of dark (clear) contrast indicate minima (maxima) in the AB signal.

In Fig. 2, a 'landscape plot' of the data is displayed: The periodicity of the AB signals survives until a voltage of about 250 mV where the electrons underneath the gate are completely depleted and the ring is effectively cut off. When both arms transmit electrons, shaded and clear areas alternate in the vertical direction, indicating oscillatory behavior as a function of the gate voltage. Attention is focused on the alternating contrast and the phase reversal when the gate voltage is increased. The smoothly changing background is identified as a residue of the total UCF signal. The phase of the AB pattern takes only the values 0 or $\pi/2$. The absence of asymmetry under field reversal $\pi/2$ is attributed to the large distance (further than 1 μ m) between the pair of current and voltage terminals on each side of the ring.

In the inset of Fig. 3, a magnetoresistance trace is displayed ($V_g = 0$ V), and the corresponding Fourier signal shows a dominant component at the single flux quantum h/e . Higher harmonics have a much reduced amplitude. The signal corresponding to total depletion ($V_g = -300$ mV) in the upper branch is plotted for comparison (square symbols).

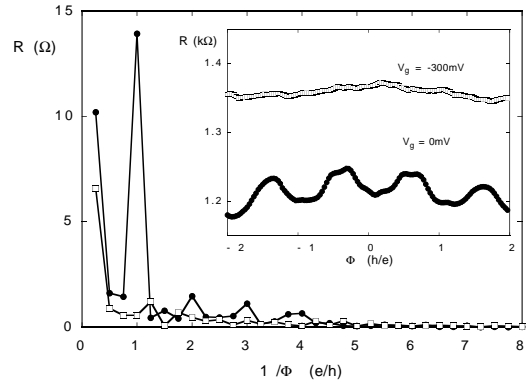


FIG. 3. Inset: Flux dependence of the sample resistance, for a closed ($V_g = 0$ V) and open ($V_g = -300$ mV) ring. Main figure: FFT transforms of these signals after subtraction of an offset.

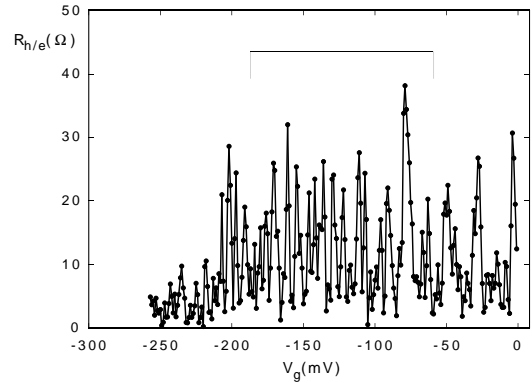


FIG. 4. Absolute value of the h/e Fourier component of the A-B resistance as function of gate voltage.

In Fig. 4, the modulus of the h/e Fourier component of the ring resistance is plotted for each value of V_g . The location of the transition between maxima and minima matches the position of the contrast changes in the pattern of the conductance landscape (Fig. 2). While the location of the resistance peaks appears to be chaotic, a detailed analysis (see below) reveals a regular structure. Peaks of reduced magnitude persist between 200 mV and the depletion voltage.

The Fourier transform of the h/e harmonic is computed for several intervals (width 128 mV), starting from different initial voltages (Fig. 5). A dominant peak at 0.062 (mV) $^{-1}$ (arrow, center of figure) corresponding to a voltage period of 16 mV appears in all intervals. Smaller peaks beyond 0.13 (mV) $^{-1}$ correspond to higher harmonics. Below 0.062 (mV) $^{-1}$, additional peaks (arrow, left of Fig. 5) are observed, which shift in position from one voltage interval to the next, from 0.037 (mV) $^{-1}$ (Fig. 5a) to 0.015 (mV) $^{-1}$ (Fig. 5d).

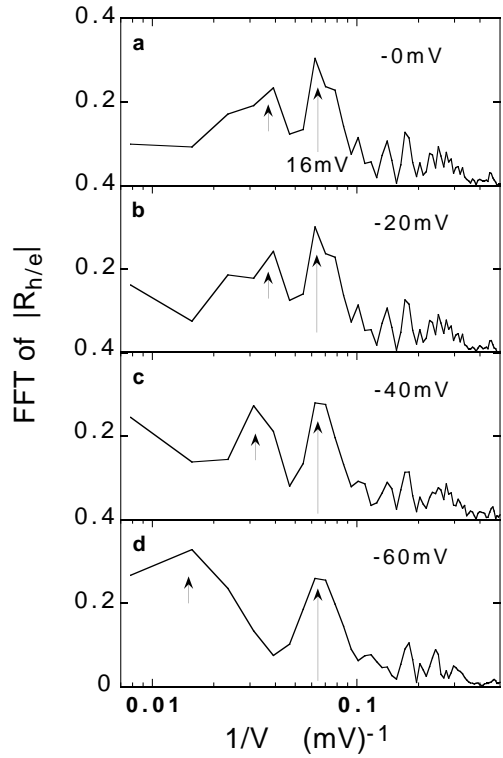


FIG. 5. The Fourier transforms of $R_{h=e}$ (FIG. 4.) over an 128mV interval for different initial voltages (a ! d) as indicated. The persistent peak corresponds to a voltage period of 16mV .

This shift reflects the changing barrier height as the mean gate voltage increases [6,7]: Oscillations, originating from several channels, correspond to an integer number of Fermi wave lengths ($2\pi(E_n/V))^{1/2}$ (E_n subband energy, V barrier height) over the length of the gate.

On the other hand, the robustness of the 16mV oscillation in all intervals signifies that it has a different origin. Lateral confinement gives rise to conductance quantization in the upper branch of the ring, and the resulting magnetoresistance signal reflects how many channels in the upper branch, contribute to the interference pattern. Between 0 and 250mV, we detect approximately 16 periodic peaks in FIG. 4. Clearly this number is lower than the estimated number of channels. Nevertheless the presence of a metallic gate induces changes in the electrical potential underneath, even at zero applied voltage (a positive voltage of a few hundred millivolts is necessary to open all channels [8]). While it is not possible to pinpoint exactly how many channels contribute to each oscillation of FIG. 4, the number of oscillations is comparable to the estimated number of transmission channels.

Theoretically, the scattering approach for coherent transport [4] predicts a conductance:

$$G = 2 \frac{e^2}{h} \sum_n j_n j_n^* ; \quad (1)$$

where the sum is taken over the transverse electron modes, and the j_n are the eigenvalues of the transmission matrix multiplied by its hermitian conjugate. The splitting of the waves between the upper and lower branch (FIG. 1), is prescribed for each mode by a 3×3 scattering matrix [13]. No reflection is assumed in the lower branch. A scatterer with a quantized conductance [14] is located on the upper branch. Phases θ_n are added to the waves crossing the gate: disorder corresponds to random phases. Electron waves are then recombined into the collecting lead, and the accumulated phase differences lead to an interference pattern. For a minimal description, no mixing between channels (backscattering) is introduced explicitly. Nevertheless, the symmetry of the S-matrix implicitly allows scattering between incoming (outgoing) channels on each side. The transmission coefficient for electrons waves in the n th channel is given by:

$$s_n = 2 \frac{p}{h} \left(\frac{1}{2} + 1 \right)^2 e^{i\theta_n} = 0 \quad (2)$$

$$1 \quad 1 \quad t_{1g}(n) t_{1g}^* = 0 \quad 1 \quad 1 \quad 1 \quad 1$$

where p controls the connection of the current probes to the ring ($p=0$ no coupling to the ring; $p=1=2$ for optimal coupling). t_1 (t_g) is a 2×2 transfer matrix describing the beam splitters on both sides of the ring (the gate which controls transmission in the upper branch). Calculations of the conductance landscape, (6 channels), are plotted in FIG. 6. In FIG. 6a ($n=0$ for all channels) the conductance pattern displays a staircase structure which results from the progressive opening/closing of the channels in the upper branch. A succession of parallel "crests" and "valleys", illustrates that the AB signals of all channels are in phase. A periodic variation of the phase shifts, $\theta_{n+1} - \theta_n = \pi/2$ [15] leads to a halving of the AB period [16] for specific voltages. Peaks of reduced size arise at these locations. The phase of the AB signal at zero bias is unperturbed.

Finally, disorder is introduced by choosing random shifts. Several configurations of disorder were tested, with the following conclusions: For a substantial depletion, peaks with a high conductance appear despite the reduction of the number of transmission channels. The phase of the AB signal alternates between the two values 0 and π when the voltage is swept. In FIG. 6b, phase shifts $[0; \pi/2; 0; 0; \pi/2]$ were picked so as to highlight the pertinent features: The landscape contains an alternation of peaks shifted by $\pi/2$ with respect to their nearest neighbors. By subtracting a linear background to FIG. 6b, a periodicity is observed in both the magnetic flux and the depletion. Finally, peak to valley variations of the conductance in FIG. 6b occur on a relatively small voltage scale (roughly 2 conductance steps of FIG. 6a).

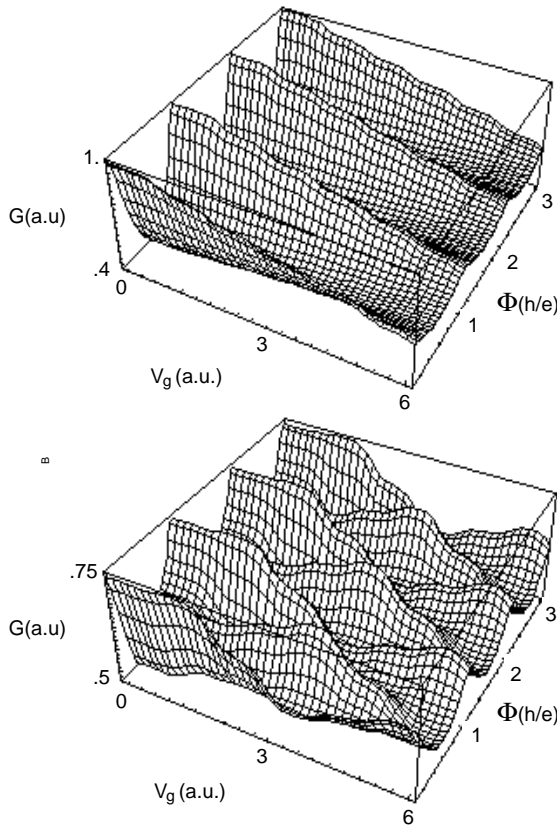


FIG. 6. a) Calculated total transmission through an Aharonov-Bohm ring with 6 modes, $n = 0$, as a function of V_g and gate voltage. b) Same calculation with channel shifts $[0; ; ; 0; 0; =2]$.

In conclusion, channel interference and conductance quantization are shown to explain the essential features of this Aharonov-Bohm experiment. When both arms are transmitting, the suppression of one single channel triggers fluctuations of the magnetoresistance which are comparable to the average signal, and may operate a shift of

of the pattern. Strikingly, the regular structure in the pattern persists from large depletion voltages, where few modes propagate in the lower branch (the typical conditions of Ref. [10]), to zero depletion voltages where most channels are transmitting. Our calculations reveal that random phase disorder must be included in the model to obtain the main features of the experiment, such as the sudden horizontal shifts of the pattern and the large variations of the AB signal when the number of channels is reduced. Physically, this phase disorder originates from variations in path lengths suffered by different modes, from geometric scattering at the beam splitters, or from inhomogeneities in the environment (impurities, etc....).

This work sheds further light on the issue of sudden phase changes in interference experiments. We speculate that this geometry can be used for the quantitative study of other scatterers located on a branch of the ring. The analysis of the resulting AB pattern then provides a way

to quantify the role of disorder and geometric scattering. Is the pattern altered significantly when the sample is heated (new impurity configuration), or it is tied primarily to the environment? In particular, it may prove interesting to study rings in which a quantum billiard is embedded. Finally, the addition of a gate to modulate the channels is also useful for the magnetic response of isolated rings. It may allow to scan through different ring configurations and therefore to vary the persistent current from a paramagnetic to a diamagnetic signal.

G.C. acknowledges support by the CNPq, Brazil.

-
- [1] D. Yu. Sharvin and Yu. V. Sharvin, Pis'ma Zh. Eksp. Teor. Fiz. 34, 285 (1981) [JETP Lett. 34, 272 (1981)].
 - [2] B.L. Altshuler, Pis'ma Zh. Eksp. Teor. Fiz. 33, 101 (1981) [JETP Lett. 33, 94 (1981)].
 - [3] R.A. Webb, S. Washburn, C.P. Umbach and R.B. Laibowitz, Phys. Rev. Lett. 54, 2692 (1985).
 - [4] M. Buttiker, Y. Imry, R. Landauer, S. Pines, Phys. Rev. B 31, 6207 (1985).
 - [5] P.A. Lee, A.D. Stone and H. Fukuyama, Phys. Rev. B 35, 1039 (1987); B.L. Altshuler, Pis'ma Zh. Eksp. Teor. Fiz. 41, 530 (1985) [JETP Lett. 41, 648 (1985)].
 - [6] S. Washburn, H. Schulz, D.P. Kern, R.A. Webb, Phys. Rev. Lett. 59, 791 (1987).
 - [7] A. Yacoby, U. Sivan, C.P. Umbach and J.M. Hong, Phys. Rev. Lett. 66, 1938 (1991); A. Yacoby et al., Phys. Rev. Lett. 73, 3149 (1994).
 - [8] D. Mailly, C. Chapelier and A. Benoit, Phys. Rev. Lett. 70, 2020 (1993).
 - [9] K.F. Berggren, G. Roos, and H. van Houten, Phys. Rev. B 37, 10118 (1988).
 - [10] B.J. van Wees et al., Phys. Rev. Lett. 60, 848 (1988); D.A. Wharam et al., J. Phys. C Solid State 21, L209 (1988).
 - [11] A. Yacoby, M. Heiblum, D. Mahalu and H. Shtrikman, Phys. Rev. Lett. 74, 4047 (1995).
 - [12] M. Buttiker, Phys. Rev. Lett. 57, 1761 (1986); A.D. Benoit, S. Washburn, C.P. Umbach, R.B. Laibowitz, R.A. Webb, ibid. 57, 1765 (1986).
 - [13] M. Buttiker, Y. Imry, M. Aibel, Phys. Rev. A 30, 1982 (1983); Y. Gefen, Y. Imry and M. Aibel, Phys. Rev. Lett. 52, 139 (1984).
 - [14] M. Buttiker, Phys. Rev. B 41, 7906 (1990); W.H. Müller, J. Phys. Chem. 48, 1651 (1968).
 - [15] G. Cemicchiaro et al. (unpublished).
 - [16] A. Yacoby, R. Schuster and M. Heiblum, Phys. Rev. B 53, 9583 (1996).